Generator and Load

Regions in the Plasma Sheet

O. Marghitu (1, 2), M. Hamrin (3), B. Klecker (2),
K. Rönnmark (3), S. Buchert (4), L.M. Kistler (5),
M. André (4), H. Rème (6)

(1) Institute for Space Sciences, Bucharest, Romania
(2) Max Planck Institute for extraterrestrial Physics, Garching, Germany
(3) Physics Department, Umeå University, Umeå, Sweden
(4) Swedish Institute of Space Physics, Uppsala, Sweden
(5) Space Science Center, University of New Hampshire, Durham, USA
(6) CESR – CNRS, Toulouse, France

Contact: marghitu@venus.nipne.ro

as Detected by Cluster

Abstract

The local conversion of mechanical energy into electromagnetic energy takes place in generator regions where $\mathbf{E} \cdot \mathbf{J} < 0$, with **E** the electric field and **J** the current density. Inside load regions the process is reversed, $\mathbf{E} \cdot \mathbf{J} > 0$, and the electromagnetic energy is converted into the mechanical energy of the plasma bulk motion and/or dissipated as heat. In this paper we concentrate on the plasma sheet, known to host both generator and load regions. Cluster offers appropriate conditions for a systematic investigation of $\mathbf{E} \cdot \mathbf{J}$ in the plasma sheet. The electric field can be inferred by using data from two instruments, CIS and EFW, which improves on the reliability of the estimates. One can also fully derive the current density vector, by using magnetic field data from the four Cluster satellites. We have scanned several plasma sheet Cluster crossings in the summer and fall of 2001 for clear $\mathbf{E} \cdot \mathbf{J}$ 0 signatures. The location of the identified generator and load regions within the plasma sheet is inferred by computing the plasma β parameter. The findings are discussed in terms of recent simulation results published in the literature and compared to previous experimental work of the authors.

Introduction

• The incentive for this study was provided by the investigation of a few generator regions in the plasma sheet boundary layer (Marghitu et al., 2006; Hamrin et al., 2006), with conjugated Cluster and FAST data.

• In order to extend the search for (auroral) generator regions we selected a time interval between the end of August and the beginning of November, 2001, with increased conjunction rate between the two spacecraft. During this time the apogee of Cluster, at 19 R_E, was in the plasma sheet, moving from midnight to the dusk.

• With the progress of the work it became clear that Cluster data can be used for a broader investigation of the energy conversion, not restricted to generator regions. Near the Cluster apogee, the conversion of magnetic energy into mechanical energy, mostly by reversible ('motor') processes, is dominant, and the plasma sheet behaves, on average, as a load. This is intuitively consistent with the expectations, in particular not far from the neutral sheet – where both the current and the electric field are on average duskward, therefore $\mathbf{E}\cdot\mathbf{J}>0$.

• Energy conversion and transport in the tail has been also studied by computer simulations, most recently by Birn and Hesse, 2005. Multi-satellite missions like Cluster allow for the direct cross-check of the data and simulation results.

Observations

Data reduction

- Selection of events that illustrate some of the features observed.
- In preparation of a systematic investigation, various quantities relevant for the energy conversion have been derived – some of them are not yet investigated in detail.
- The tetrahedron geometry is appropriate to apply the Curlometer, with planarity and elongation less than 0.1.
- CODIF and HIA data (not shown) are averaged over 24 s. EFW data, obtained by spin fit, has 4 s resolution.
- The energy conversion regions are best visible in the cumulative sum of **E•J**. Because of the different time resolution, the cumulative sum with EFW data is (ideally about 6 times) larger.
- From EFW we only use the cumulative sum of $E_y J_y$, to validate the particle based results. E_x is (most of the time) very small, and E_z cannot be determined from EFW data, in the tail.

- The agreement between CODIF, EFW, and HIA is often quite good, which is remarkable given the completely different types of data.

Loads

- Energy conversion is dominated by loads (L1–L5), most of which are associated with bulk flow (mainly field aligned), often also with temperature anisotropy ($T_\parallel > T_\perp$).
- Bulk flow, however, is not necessarily associated with loads (L1d, L2d).
- Big loads (L2c, L3d) are often seen near midnight, close to the neutral sheet (high β). No significant load is observed, in this region when the bulk flow is missing (L2a, L2b, L3a, L3b, L3c).
- Small and moderate loads (L1b, L1c, L4c, L4d, L5b) are observed near the plasma sheet boundary (low beta).
- Moderate loads observed also close to the neutral sheet, when away from midnight (L5a).

• Some correlation between the load magnitude and AE (not shown).

• Both concentrated (L1–L5) and distributed loads (not shown). The distributed loads do not appear to be associated with bulk flow.

Generators

• Less numerous, and less intense (G1, G2).

• Observed mainly away from the midnight and close to the plasma sheet boundary (G1a–d).

• Both concentrated (G1) and distributed (G2) generator regions.

• As for the loads, the concentrated generator regions (CGRs) appear to be associated with bulk flow and temperature anizotropy. This does not seem to hold for for the distributed generator regions.

• Poynting flux is emitted from the CGRs and possibly makes it to the aurora.

• Detailed analysis of G1a–d in Marghitu et al., 2006, and Hamrin et al., 2006.

L1

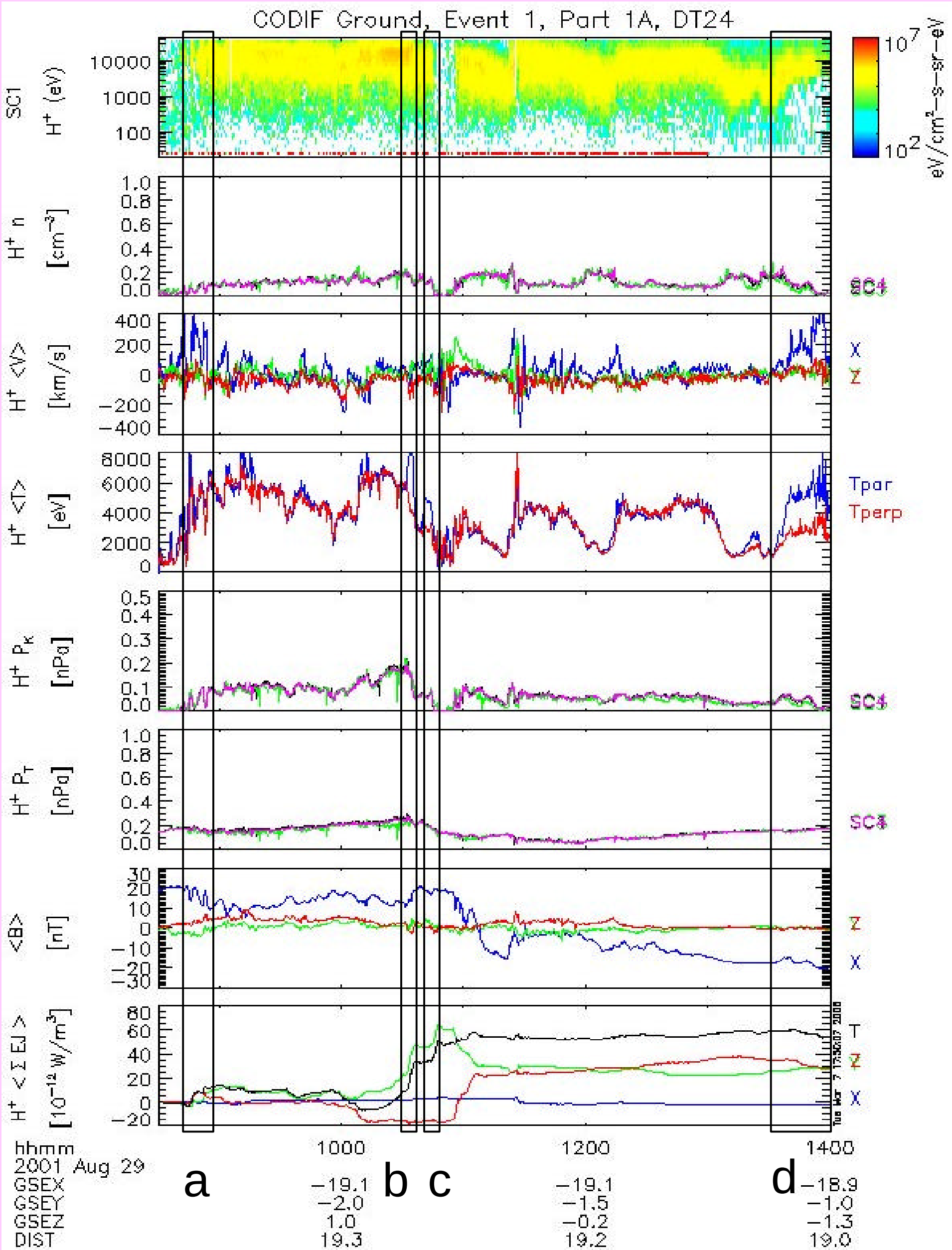
CODIF Ground, Event 1, Part 1A, DT24
SC1 H+ (eV)
H+ n [cm-3]
H+ <V> [km/s]
H+ <T> [eV]
Tpar
Tperp
H+ PK [nPa]
H+ PT [nPa]
<B> [nT]
H+ < Σ EJ > [10-12 W/m3]
hhmm
2001 Aug 29
GSEX
GSEY
GSEZ
DIST
a
b
c
d

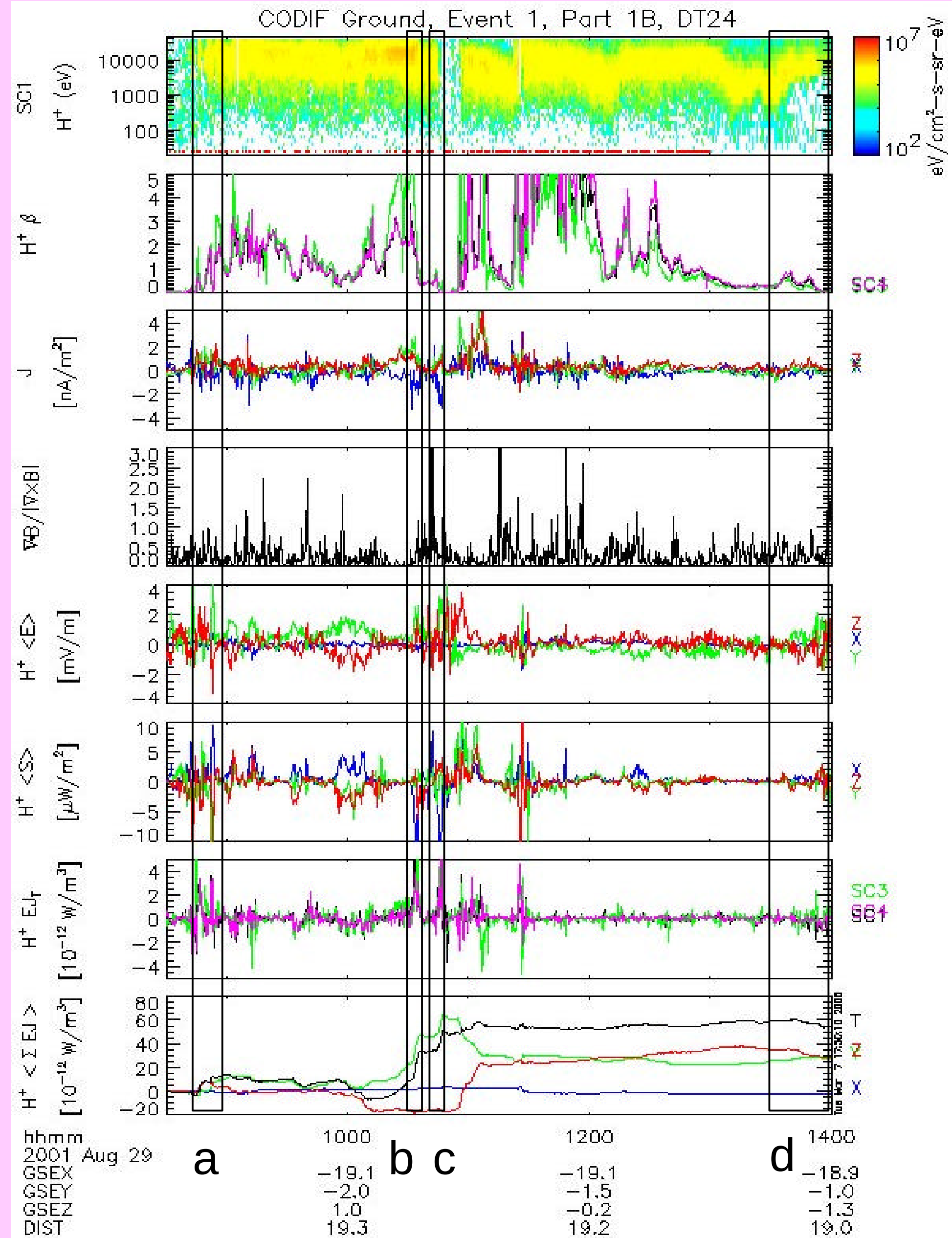
CODIF Ground, Event 1, Part 1B, DT24
SC1 H+ (eV)
H+ β
J [nA/m2]
∇B/|∇×B|
H+ <E> [mV/m]
H+ <S> [μW/m2]
H+ EJT [10-12 W/m3]
H+ < Σ EJ > [10-12 W/m3]
hhmm
2001 Aug 29
GSEX
GSEY
GSEZ
DIST
a
b
c
d

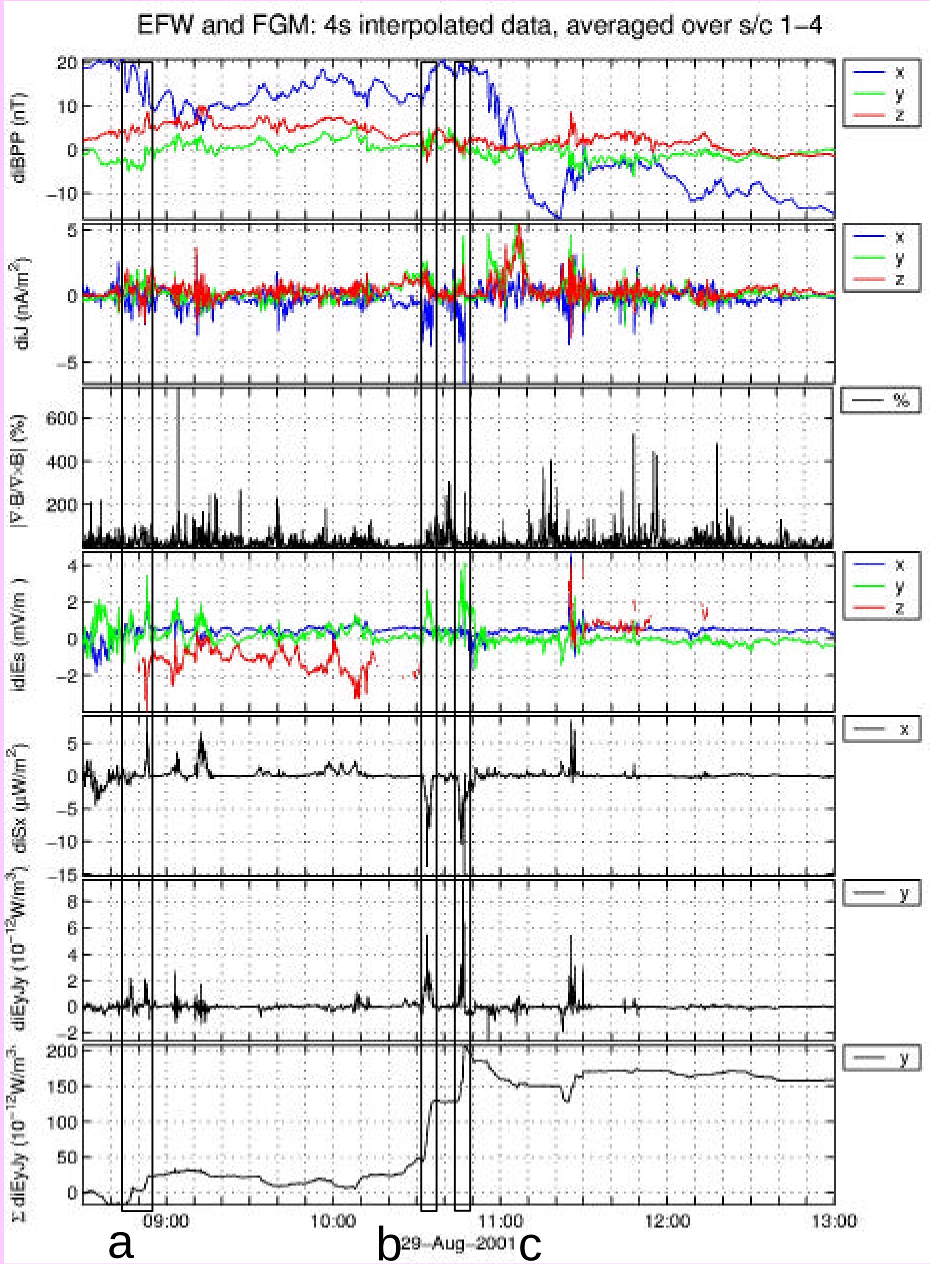
EFW and FGM: 4s interpolated data, averaged over s/c 1−4
diBPP (nT)
diJ (nA/m²)
|∇·B|/|∇×B| (%)
idiEs (mV/m)
diSx (μW/m²)
diEy.Jy (10⁻¹²W/m³)
Σ diEy.Jy (10⁻¹²W/m³)
x
y
z
%
09:00
10:00
11:00
12:00
13:00
29−Aug−2001
a
b
c

L2

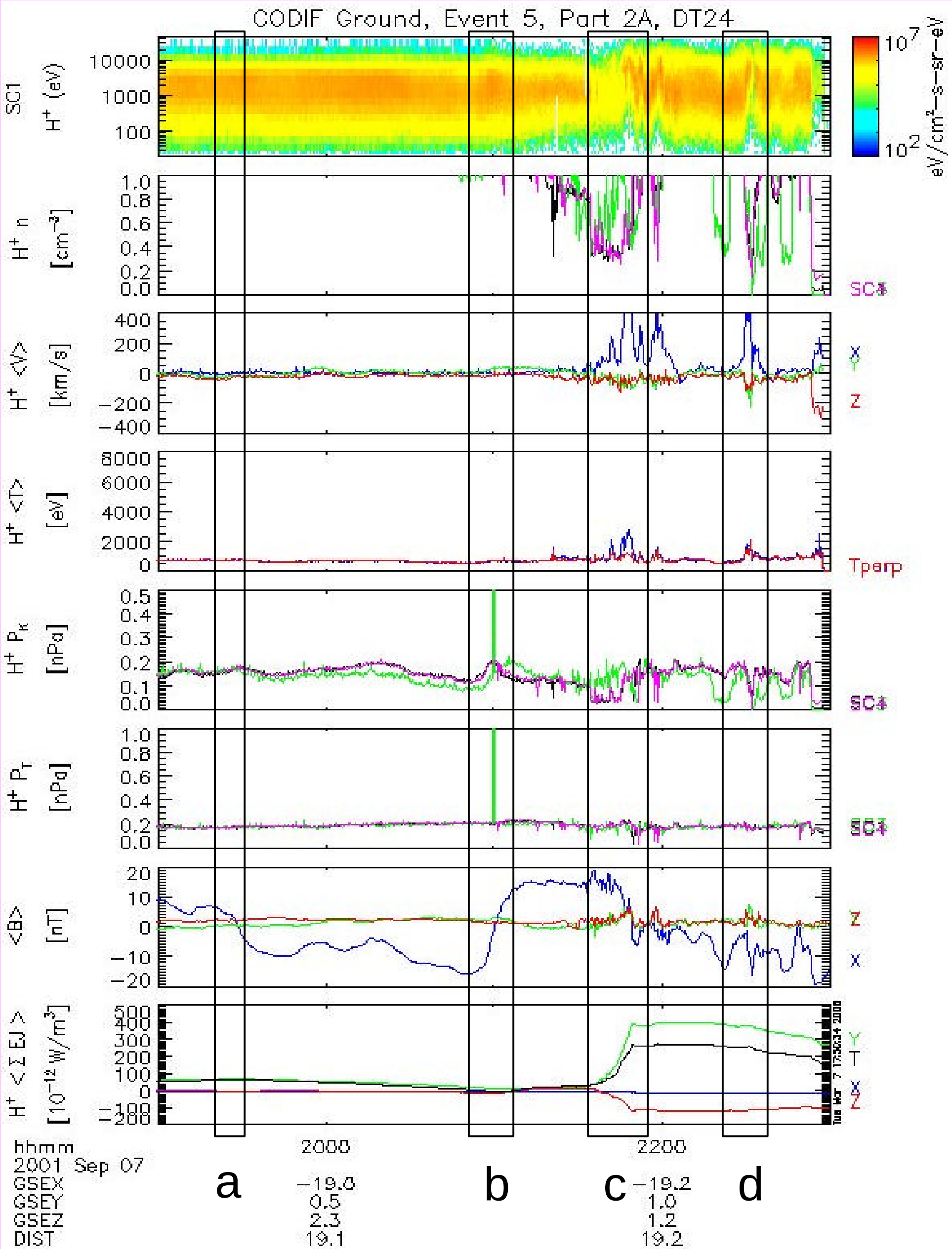
CODIF Ground, Event 5, Part 2A, DT24
SC1 H+ (eV)
eV/cm2-s-sr-eV
H+ n [cm-3]
H+ <V> [km/s]
H+ <T> [eV]
Tparp
H+ PK [nPa]
H+ PT [nPa]
<B> [nT]
H+ <Σ EJ> [10-12 W/m3]
hhmm
2001 Sep 07
GSEX −19.0 −19.2
GSEY 0.5 1.0
GSEZ 2.3 1.2
DIST 19.1 19.2
2000
2200
a
b
c
d

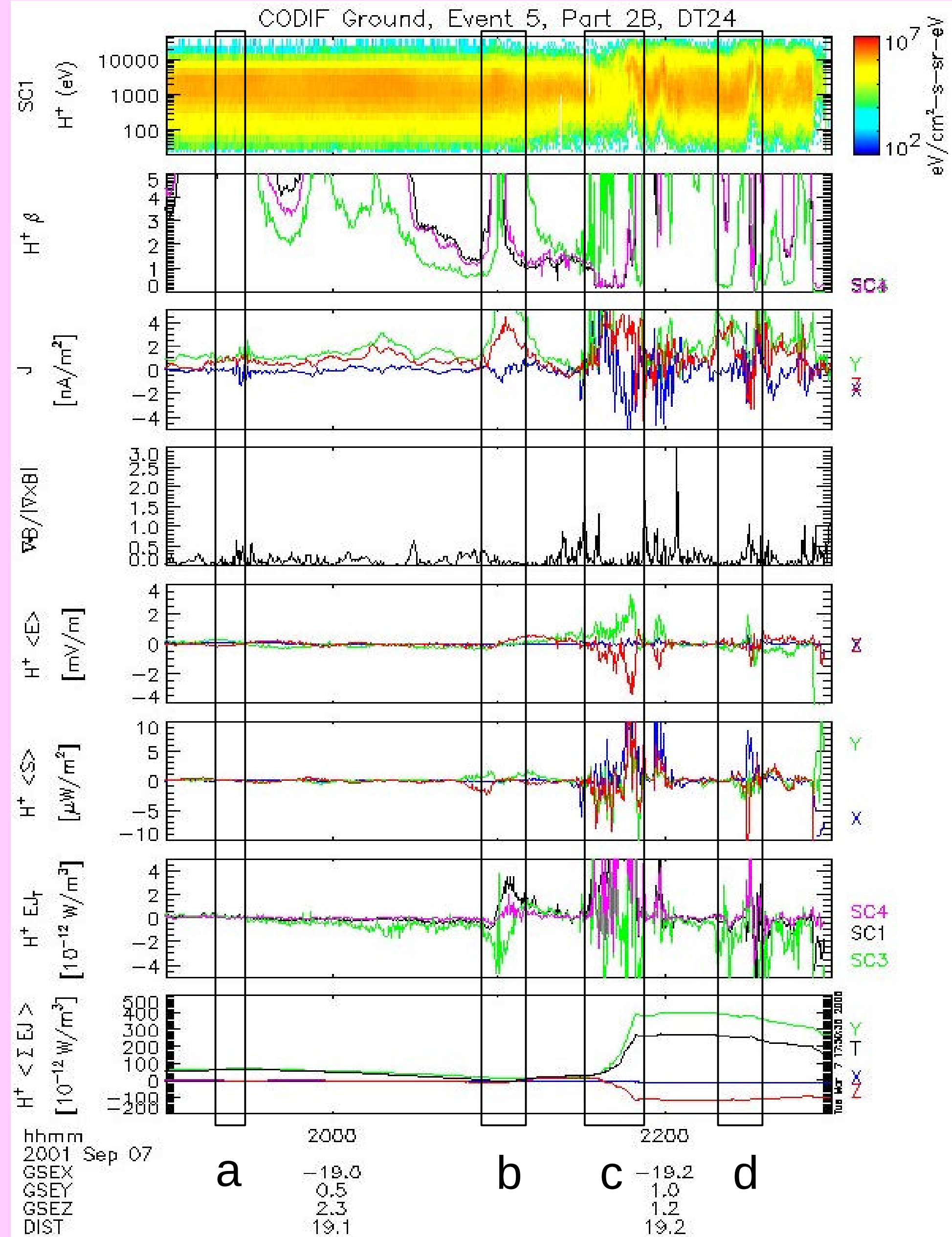
CODIF Ground, Event 5, Part 2B, DT24
SC1 H+ (eV)
eV/cm2-s-sr-eV
H+ β
J [nA/m2]
∇·B/|∇×B|
H+ <E> [mV/m]
H+ <S> [μW/m2]
H+ EJT [10-12 W/m3]
SC4
SC1
SC3
H+ <Σ EJ> [10-12 W/m3]
hhmm
2001 Sep 07
GSEX −19.0 −19.2
GSEY 0.5 1.0
GSEZ 2.3 1.2
DIST 19.1 19.2
2000
2200
a
b
c
d

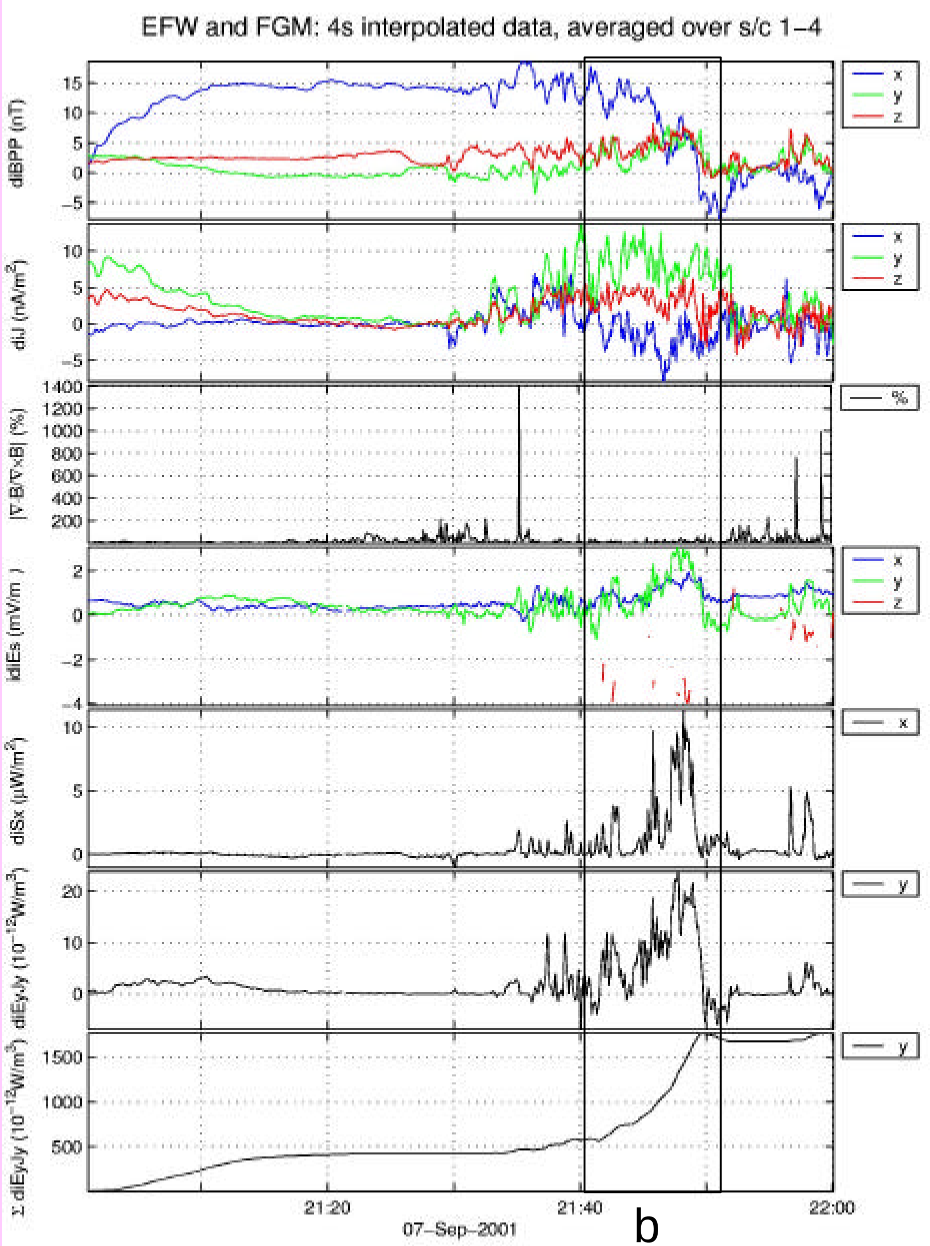
EFW and FGM: 4s interpolated data, averaged over s/c 1−4
diBPP (nT)
diJ (nA/m^2)
|∇·B/∇×B| (%)
diEs (mV/m)
diSx (μW/m^2)
diEy.Jy (10^-12 W/m^3)
Σ diEyJy (10^-12 W/m^3)
x
y
z
%
21:20
21:40
22:00
07−Sep−2001

b

L3

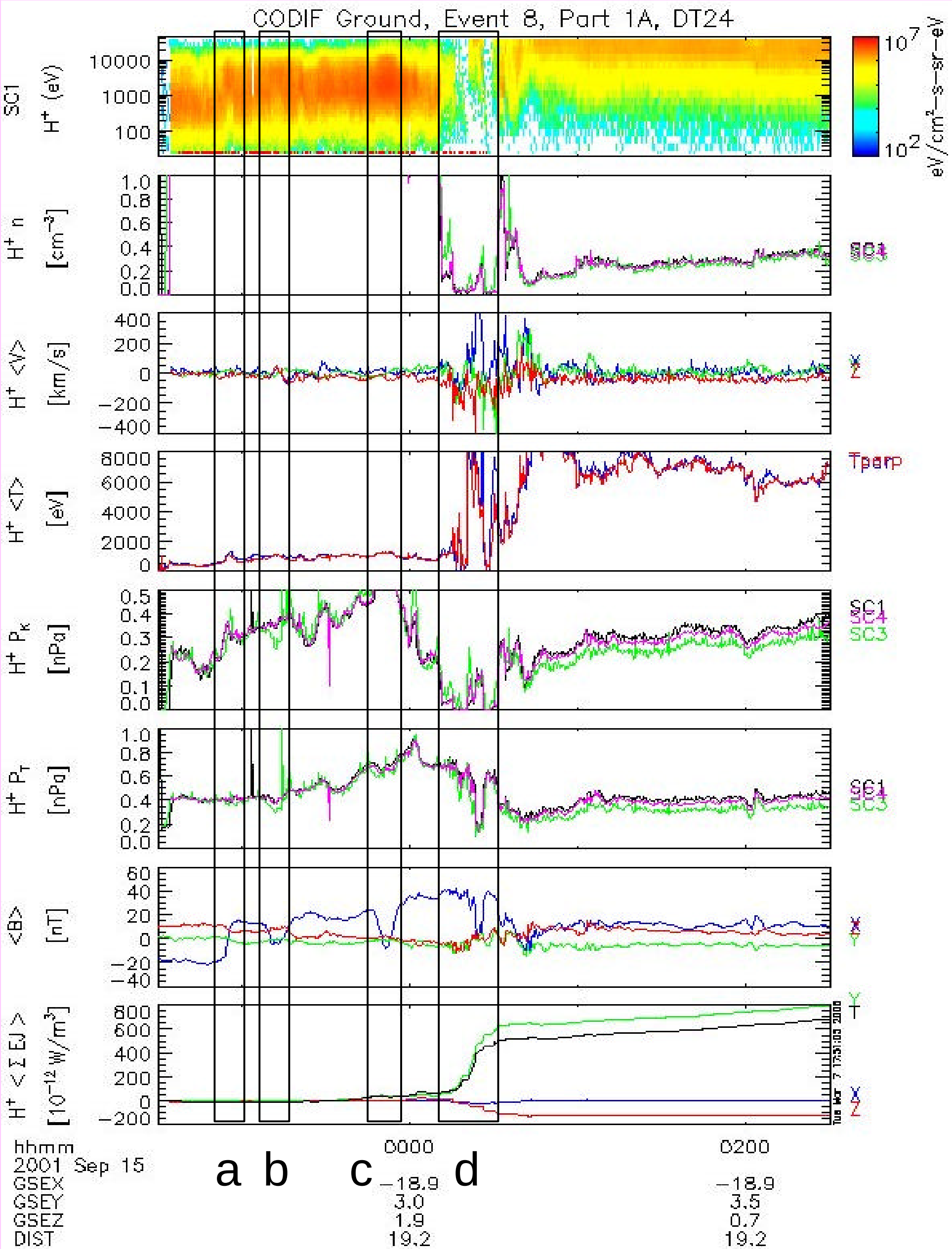
CODIF Ground, Event 8, Part 1A, DT24
SC1
H+ (eV)
eV/cm2-s-sr-eV
H+ n [cm-3]
SC4
H+ <V> [km/s]
X
Z
H+ <T> [eV]
Tperp
H+ PK [nPa]
SC1
SC4
SC3
H+ PT [nPa]
SC1
SC3
<B> [nT]
X
Y
H+ <Σ EJ> [10-12 W/m3]
Y
T
X
Z
hhmm
2001 Sep 15
GSEX
GSEY
GSEZ
DIST
0000
-18.9
3.0
1.9
19.2
0200
-18.9
3.5
0.7
19.2
a
b
c
d

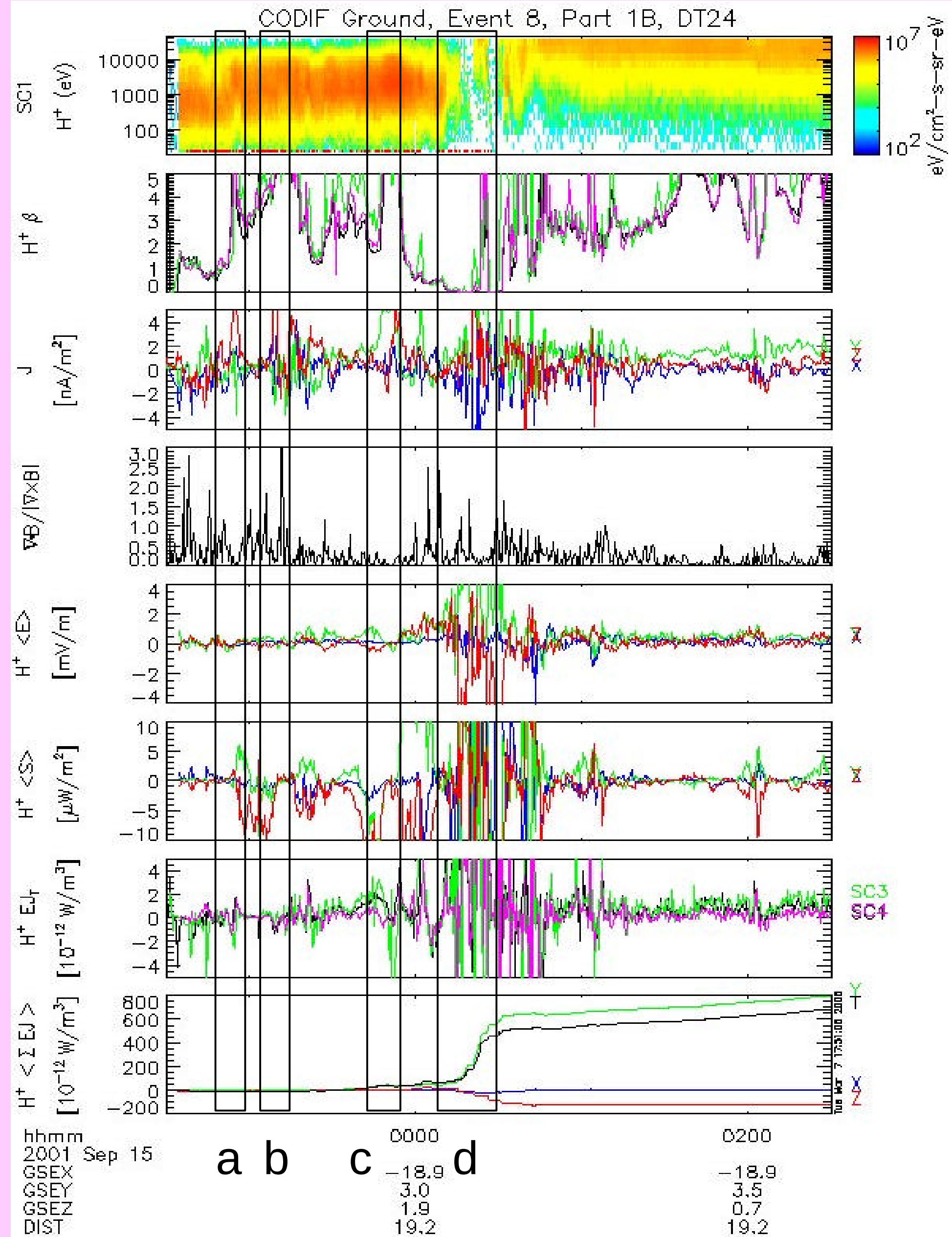
CODIF Ground, Event 8, Part 1B, DT24
SC1
H+ (eV)
eV/cm2-s-sr-eV
H+ β
J [nA/m2]
Y
Z
X
∇B/|∇×B|
H+ <E> [mV/m]
H+ <S> [μW/m2]
H+ EJT [10-12 W/m3]
SC3
SC4
H+ <Σ EJ> [10-12 W/m3]
Y
T
X
Z
hhmm
2001 Sep 15
GSEX
GSEY
GSEZ
DIST
0000
-18.9
3.0
1.9
19.2
0200
-18.9
3.5
0.7
19.2
a
b
c
d

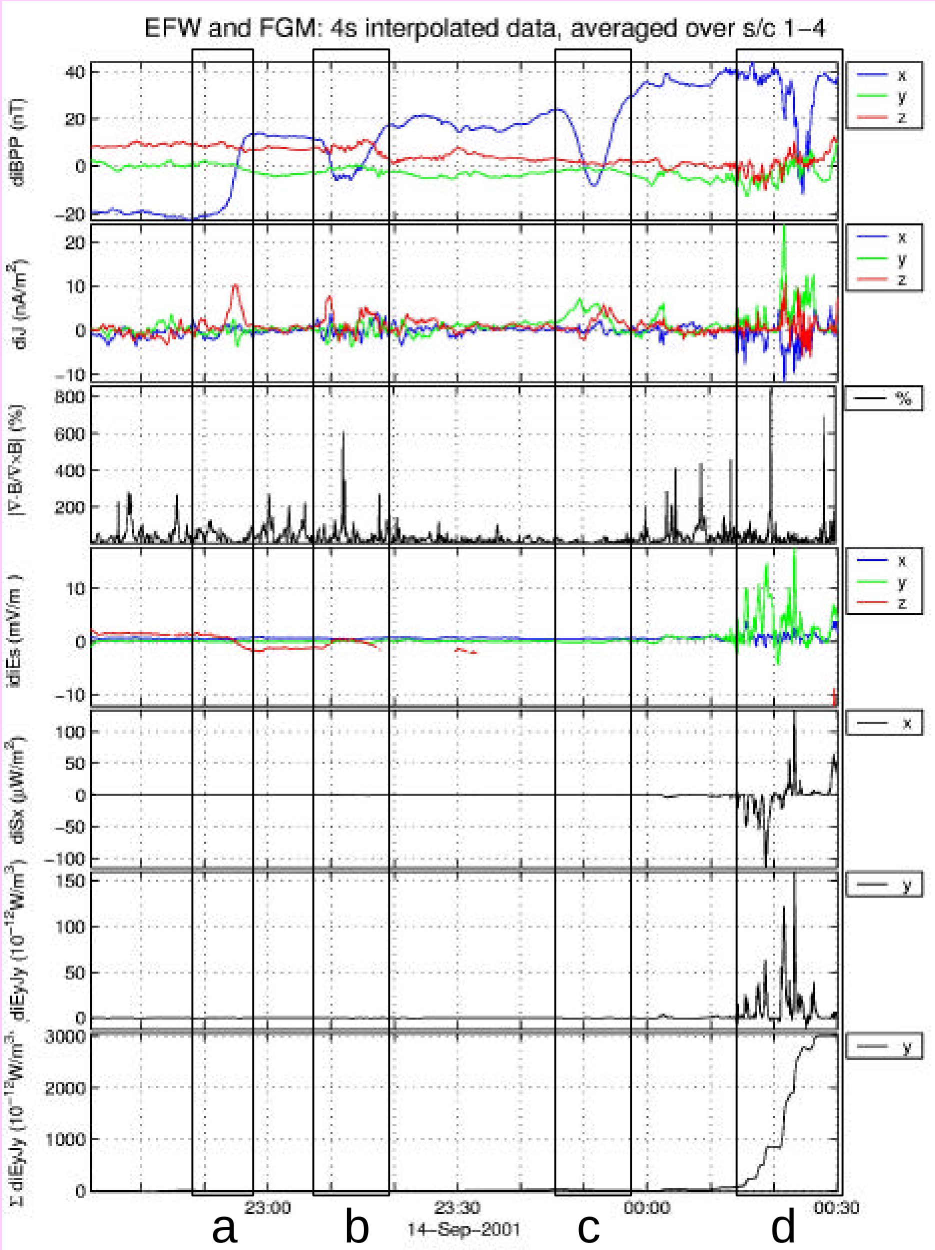

EFW and FGM: 4s interpolated data, averaged over s/c 1–4
diBPP (nT)
diJ (nA/m^2)
|∇·B/∇×B| (%)
idiEs (mV/m)
diSx (μW/m^2)
diEyJy (10^{-12}W/m^3)
Σ diEyJy (10^{-12}W/m^3)
x
y
z
%
23:00
23:30
00:00
00:30
14–Sep–2001
a
b
c
d

L4

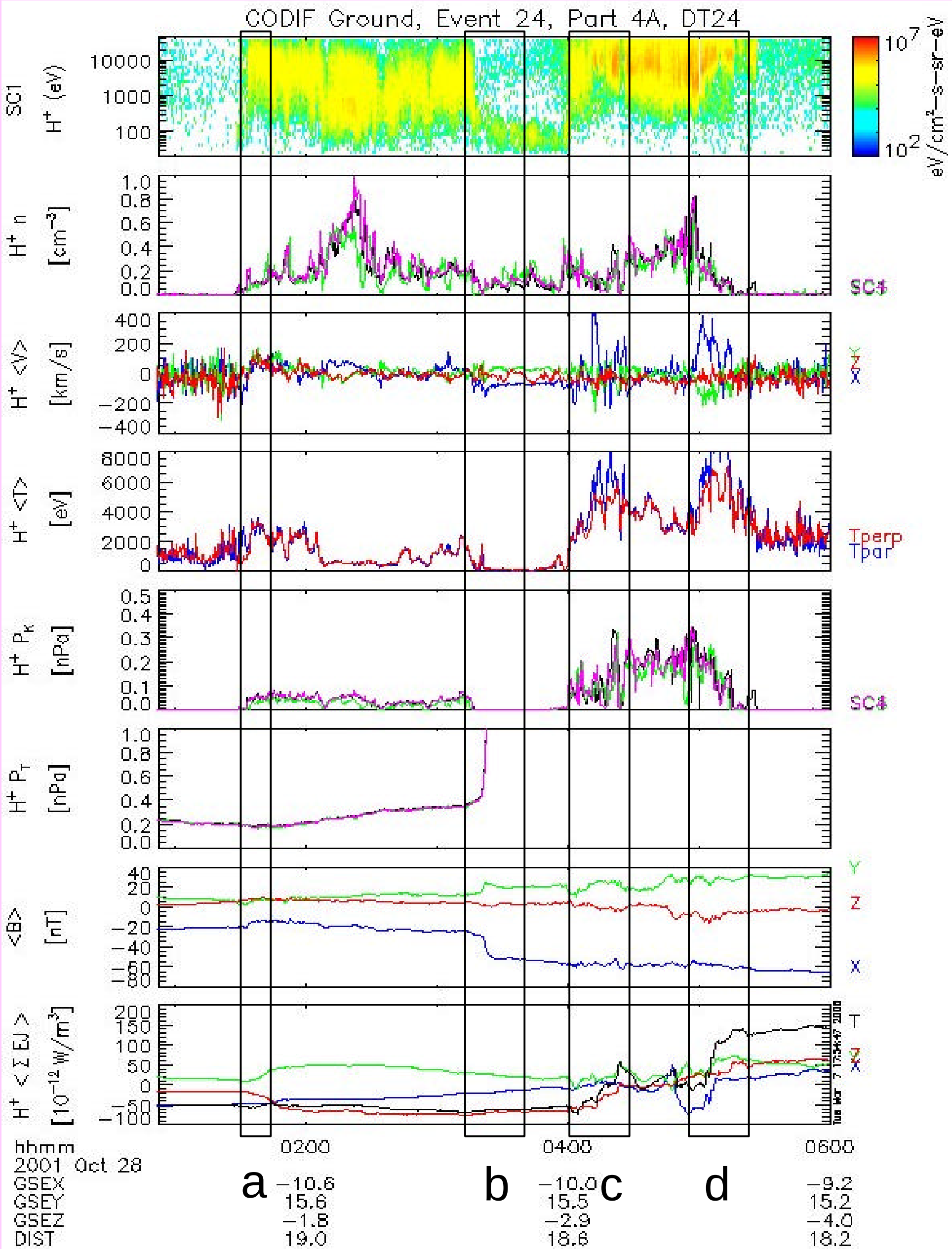
CODIF Ground, Event 24, Part 4A, DT24
SC1 H+ (eV)
eV/cm2-s-sr-eV
H+ n [cm-3]
H+ <V> [km/s]
H+ <T> [eV]
Tperp
Tpar
H+ PK [nPa]
H+ PT [nPa]
<B> [nT]
H+ < Σ EJ > [10-12 W/m3]
hhmm
2001 Oct 28
GSEX
GSEY
GSEZ
DIST
0200
0400
0600
a
b
c
d
-10.6
15.6
-1.8
19.0
-10.0
15.5
-2.9
18.6
-9.2
15.2
-4.0
18.2

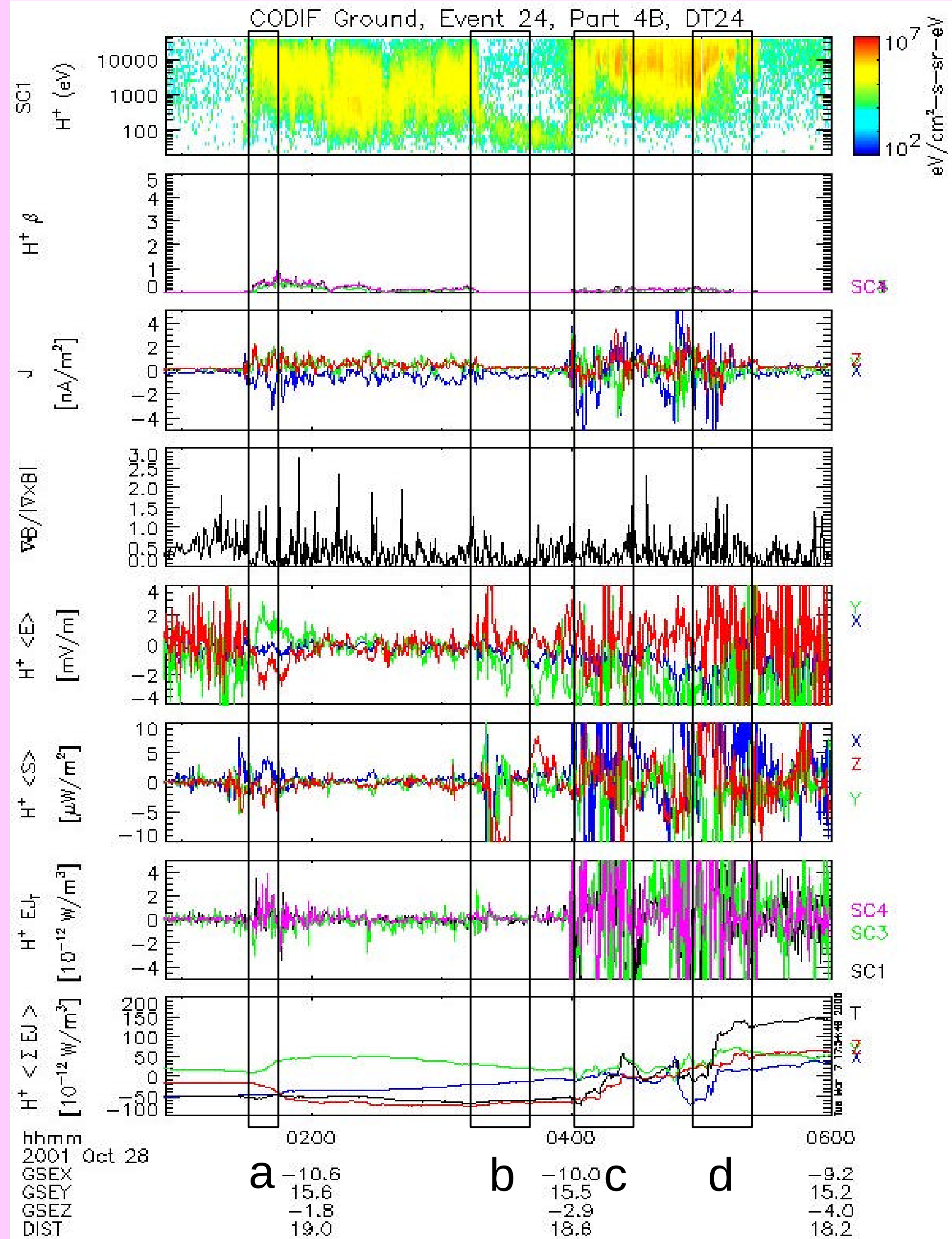
CODIF Ground, Event 24, Part 4B, DT24
SC1 H+ (eV)
eV/cm2-s-sr-eV
H+ β
J [nA/m2]
∇B/|∇×B|
H+ <E> [mV/m]
H+ <S> [μW/m2]
H+ EJT [10-12 W/m3]
SC4
SC3
SC1
H+ < Σ EJ > [10-12 W/m3]
hhmm
2001 Oct 28
GSEX
GSEY
GSEZ
DIST
0200
0400
0600
a
b
c
d
-10.6
15.6
-1.8
19.0
-10.0
15.5
-2.9
18.6
-9.2
15.2
-4.0
18.2

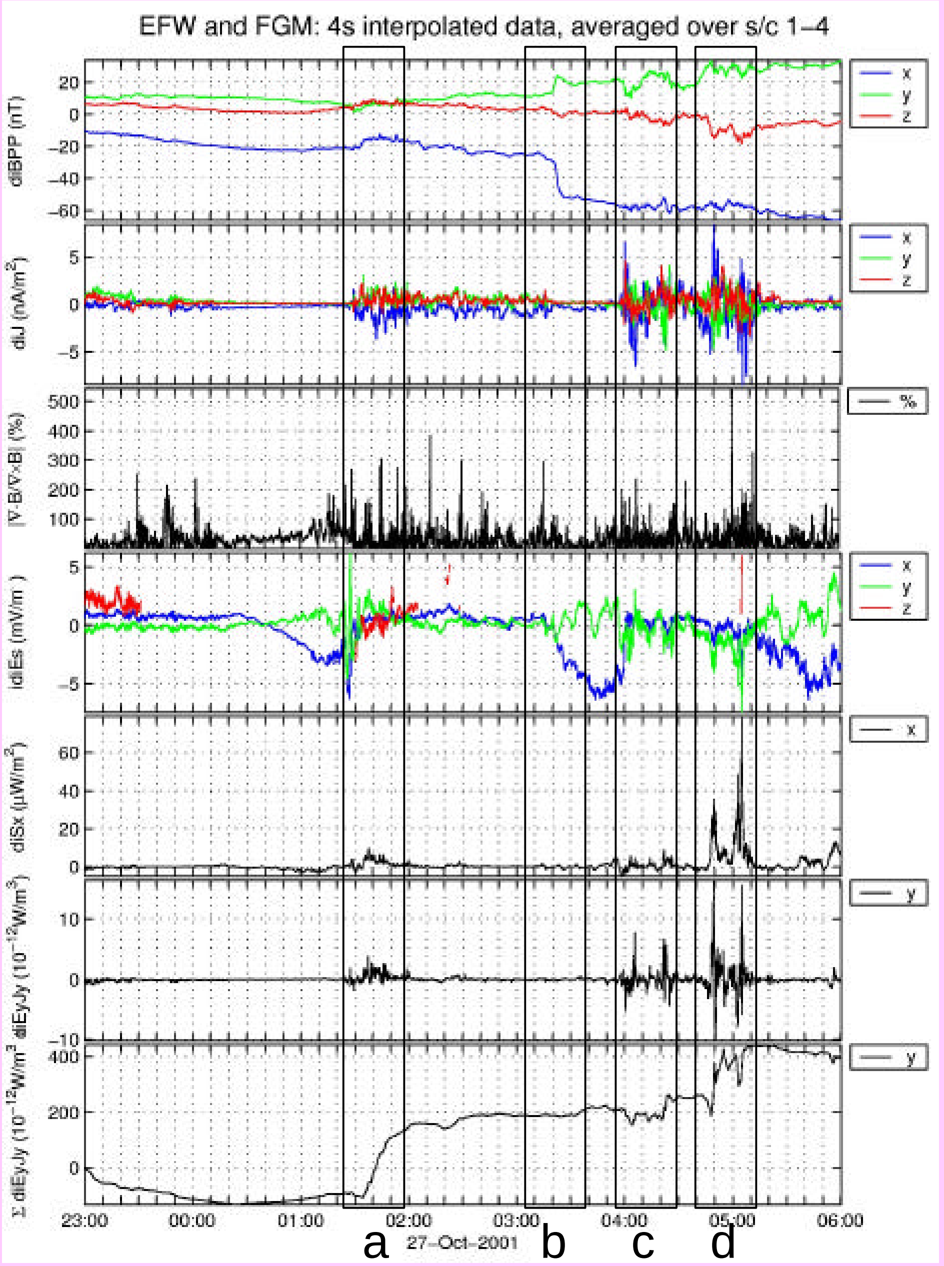

EFW and FGM: 4s interpolated data, averaged over s/c 1–4
diBPP (nT)
diJ (nA/m²)
|∇·B/∇×B| (%)
|diEs (mV/m)
diSx (µW/m²)
diEyJy (10⁻¹²W/m³)
Σ diEyJy (10⁻¹²W/m³)
23:00
00:00
01:00
02:00
03:00
04:00
05:00
06:00
27–Oct–2001
a
b
c
d

L5

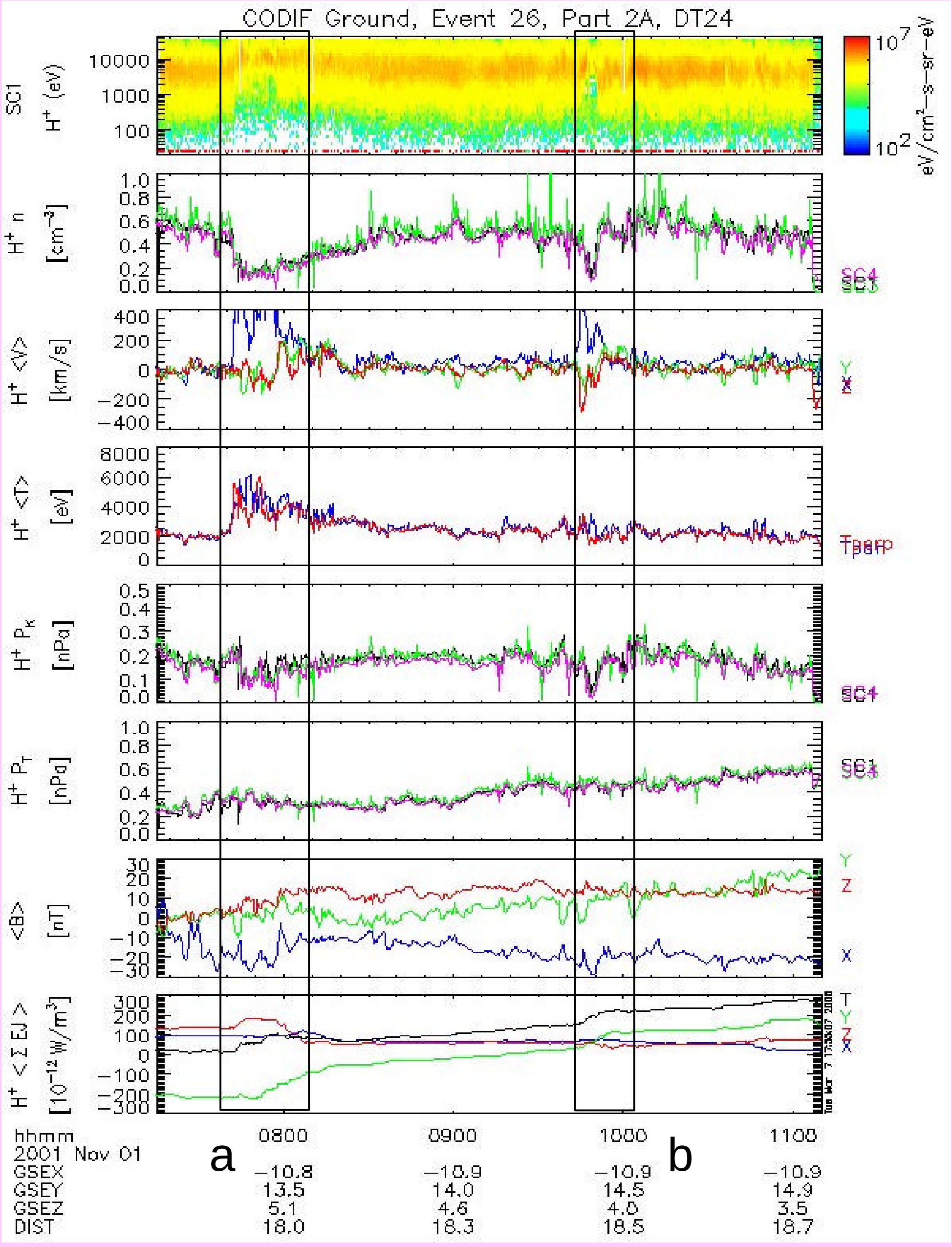
CODIF Ground, Event 26, Part 2A, DT24
SC1 H+ (eV)
eV/cm2-s-sr-eV
H+ n [cm-3]
H+ <V> [km/s]
H+ <T> [eV]
Tperp
Tpar
H+ PK [nPa]
H+ PT [nPa]
<B> [nT]
H+ <Σ EJ> [10-12 W/m3]
SC4
SC1
Y
Z
X
T
hhmm
2001 Nov 01
GSEX
GSEY
GSEZ
DIST
0800
0900
1000
1100
-10.8
-10.9
-10.9
-10.9
13.5
14.0
14.5
14.9
5.1
4.6
4.0
3.5
18.0
18.3
18.5
18.7
a
b

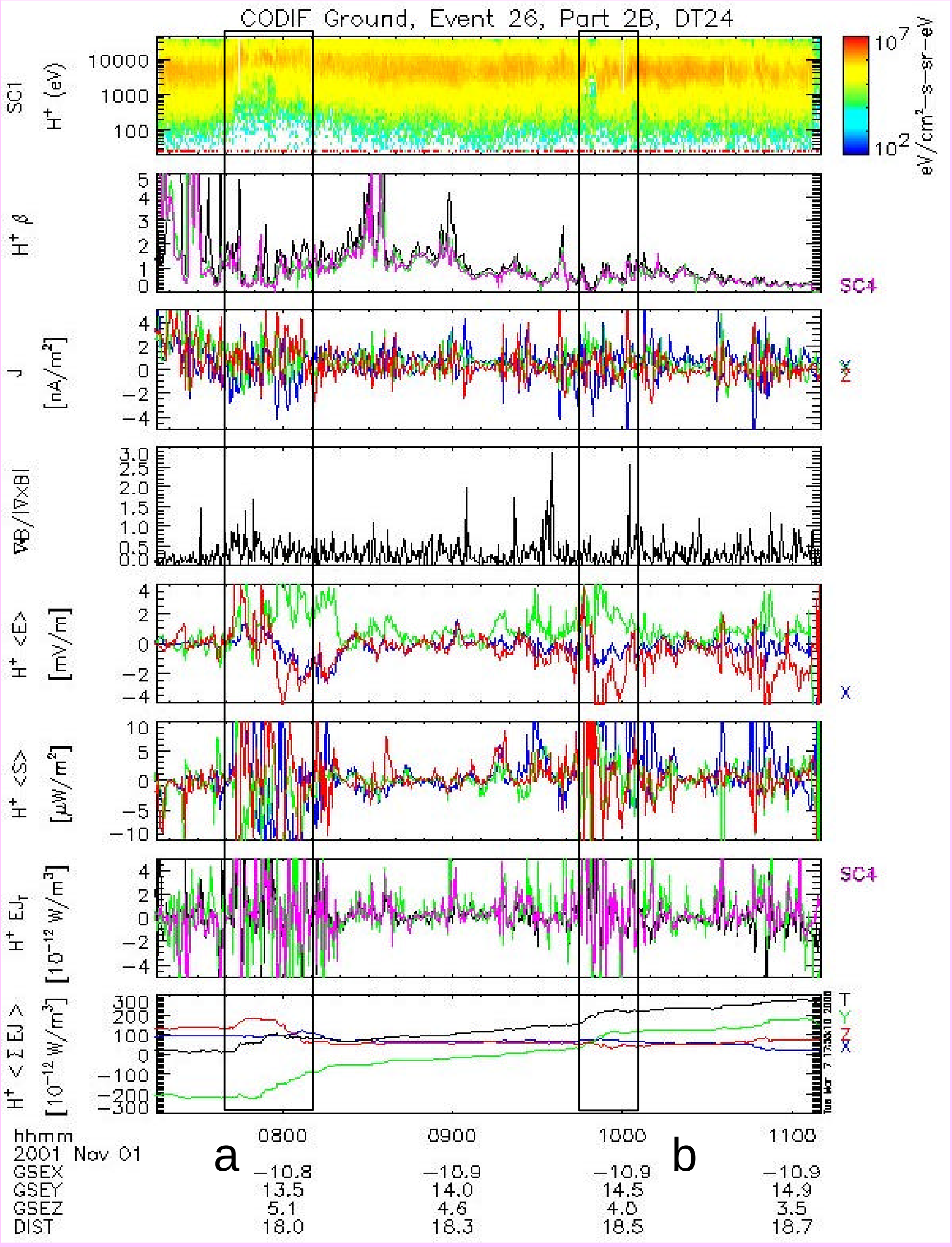
CODIF Ground, Event 26, Part 2B, DT24
SC1 H+ (eV)
eV/cm2-s-sr-eV
H+ β
J [nA/m2]
∇B/|∇×B|
H+ <E> [mV/m]
H+ <S> [μW/m2]
H+ EJT [10-12 W/m3]
H+ <Σ EJ> [10-12 W/m3]
SC4
X
Z
Y
T
hhmm
2001 Nov 01
GSEX
GSEY
GSEZ
DIST
0800
0900
1000
1100
-10.8
-10.9
-10.9
-10.9
13.5
14.0
14.5
14.9
5.1
4.6
4.0
3.5
18.0
18.3
18.5
18.7
a
b

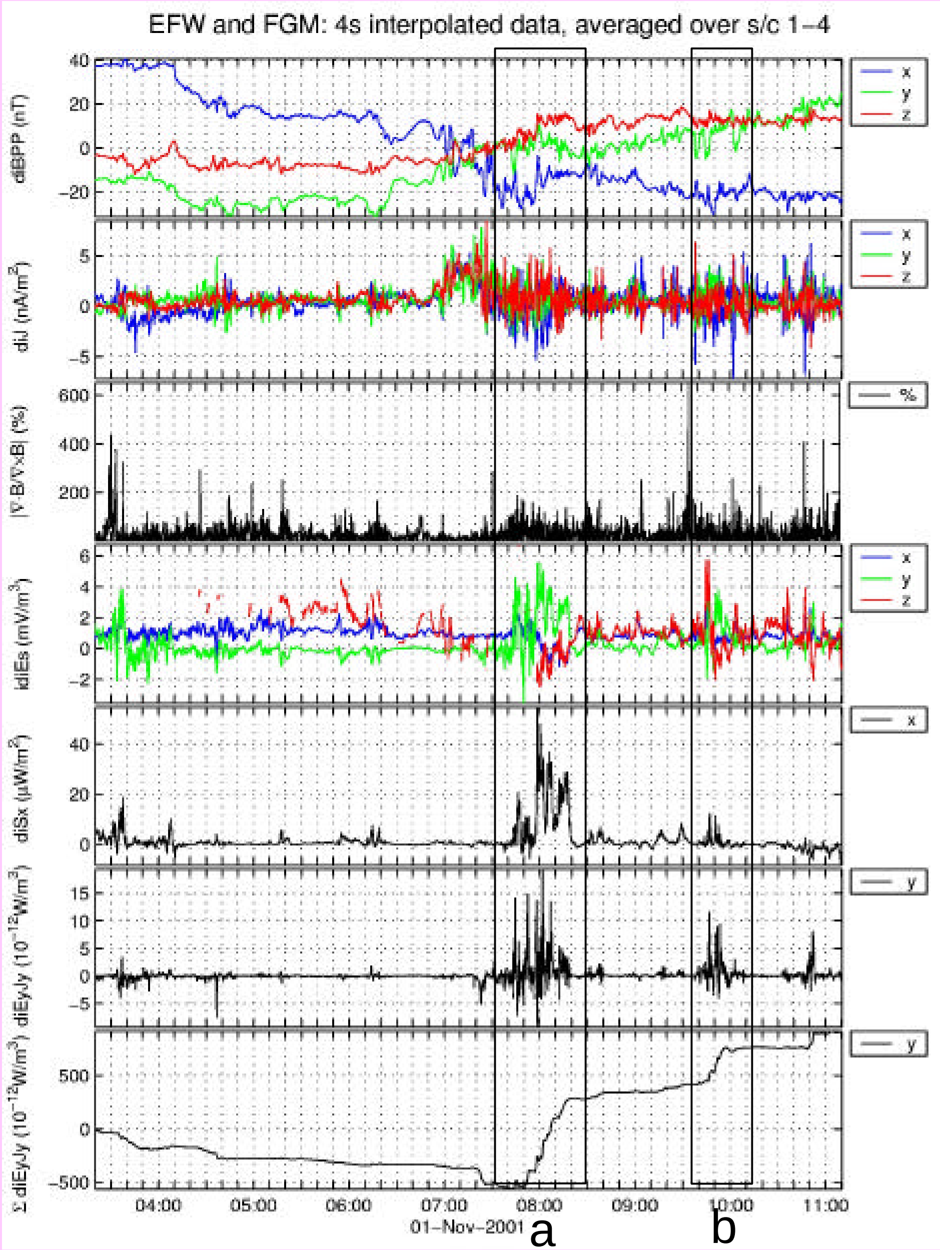

EFW and FGM: 4s interpolated data, averaged over s/c 1–4
diBPP (nT)
diJ (nA/m^2)
$|\nabla \cdot B / \nabla \times B|$ (%)
idiEs (mV/m^3)
diSx (μW/m^2)
diEyJy (10^{-12}W/m^3)
Σ diEyJy (10^{-12}W/m^3)
04:00
05:00
06:00
07:00
08:00
09:00
10:00
11:00
01–Nov–2001
a
b

G1

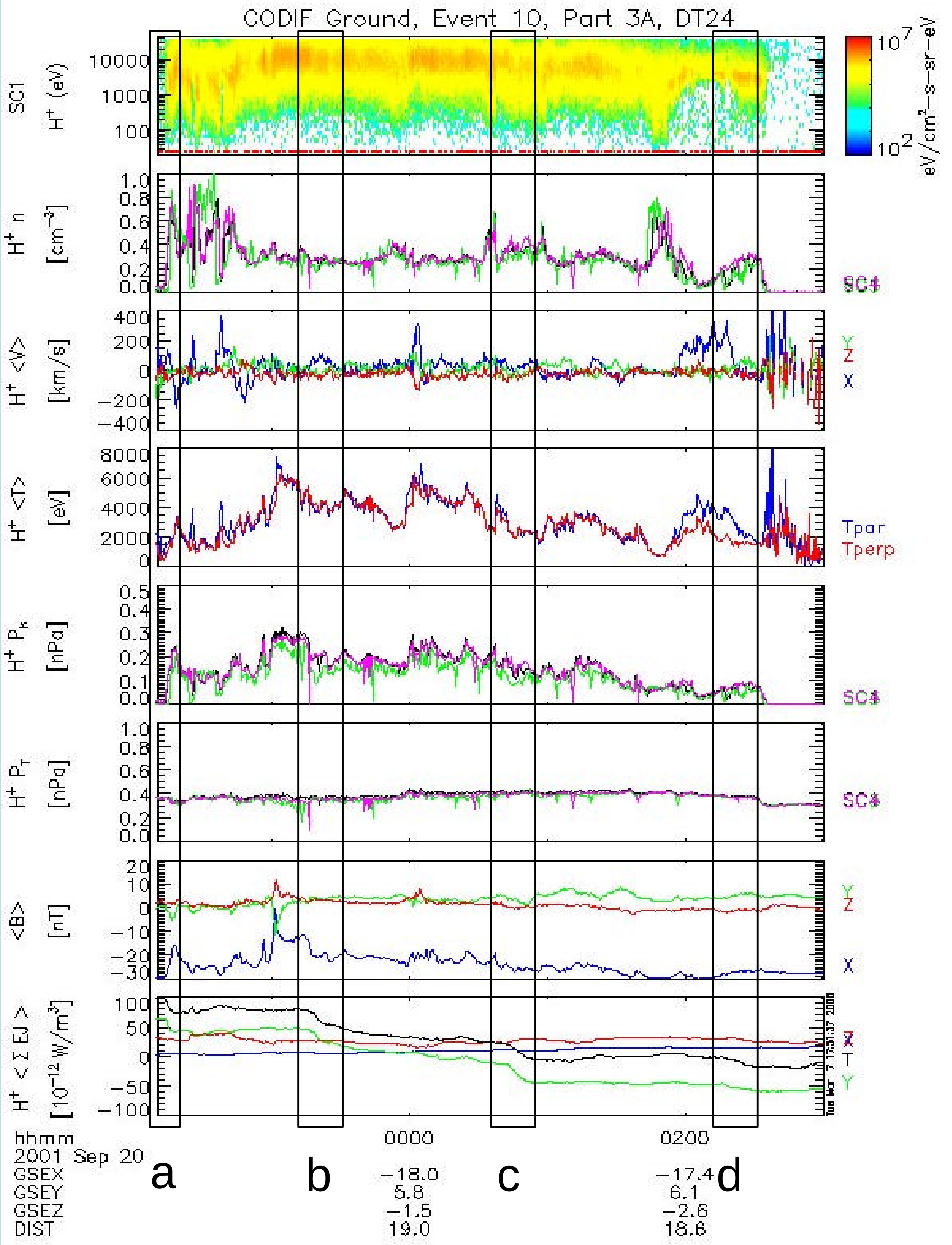
CODIF Ground, Event 10, Part 3A, DT24
SC1
H+ (eV)
eV/cm2-s-sr-eV
H+ n [cm-3]
H+ <V> [km/s]
H+ <T> [eV]
Tpar
Tperp
H+ PK [nPa]
H+ PT [nPa]
<B> [nT]
H+ <Σ EJ> [10-12 W/m3]
hhmm
2001 Sep 20
GSEX
GSEY
GSEZ
DIST
0000
-18.0
5.8
-1.5
19.0
0200
-17.4
6.1
-2.6
18.6
a
b
c
d

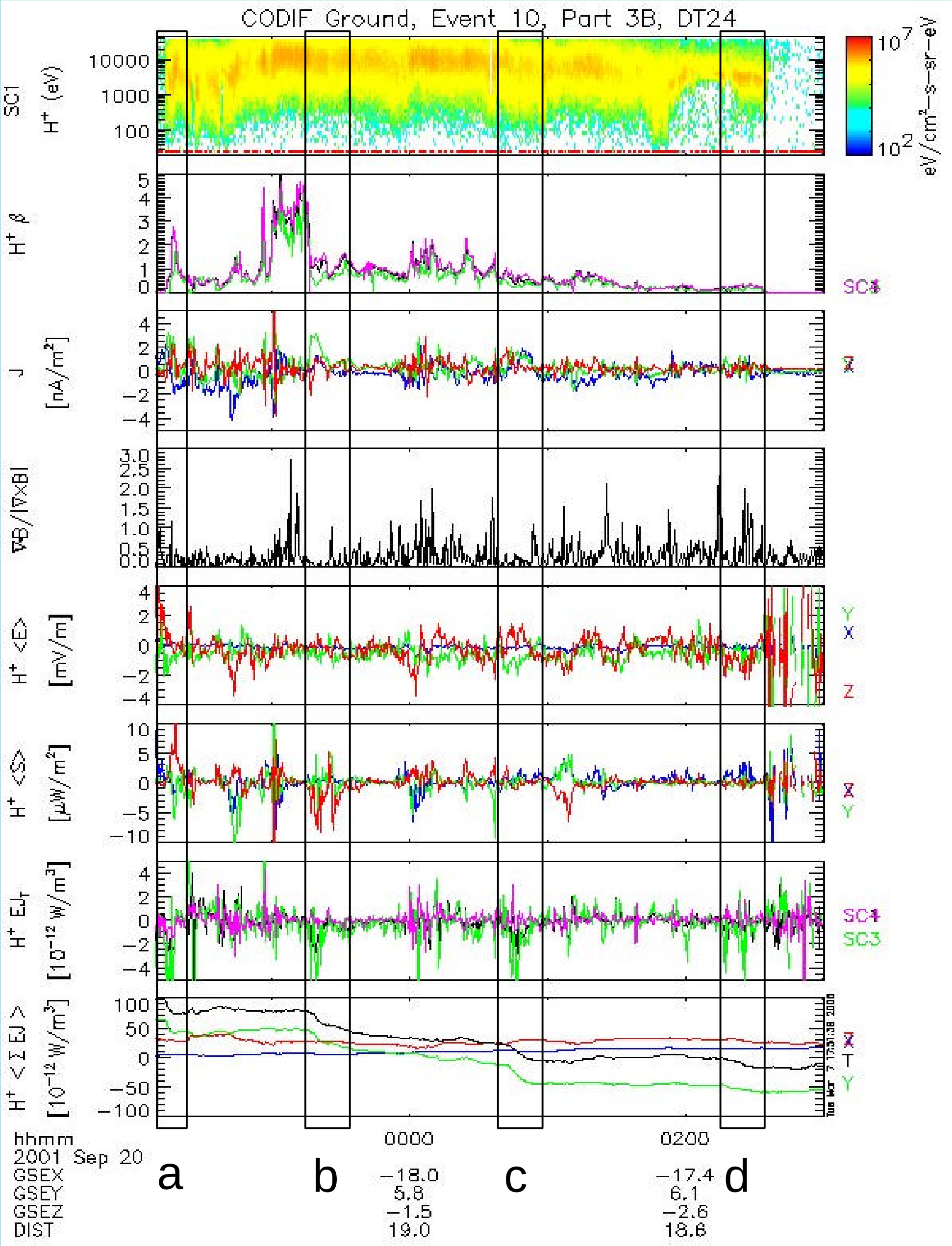
CODIF Ground, Event 10, Part 3B, DT24
SC1
H+ (eV)
eV/cm2-s-sr-eV
H+ β
J [nA/m2]
∇B/|∇×B|
H+ <E> [mV/m]
H+ <S> [μW/m2]
H+ EJT [10-12 W/m3]
SC3
H+ <Σ EJ> [10-12 W/m3]
hhmm
2001 Sep 20
GSEX
GSEY
GSEZ
DIST
0000
-18.0
5.8
-1.5
19.0
0200
-17.4
6.1
-2.6
18.6
a
b
c
d

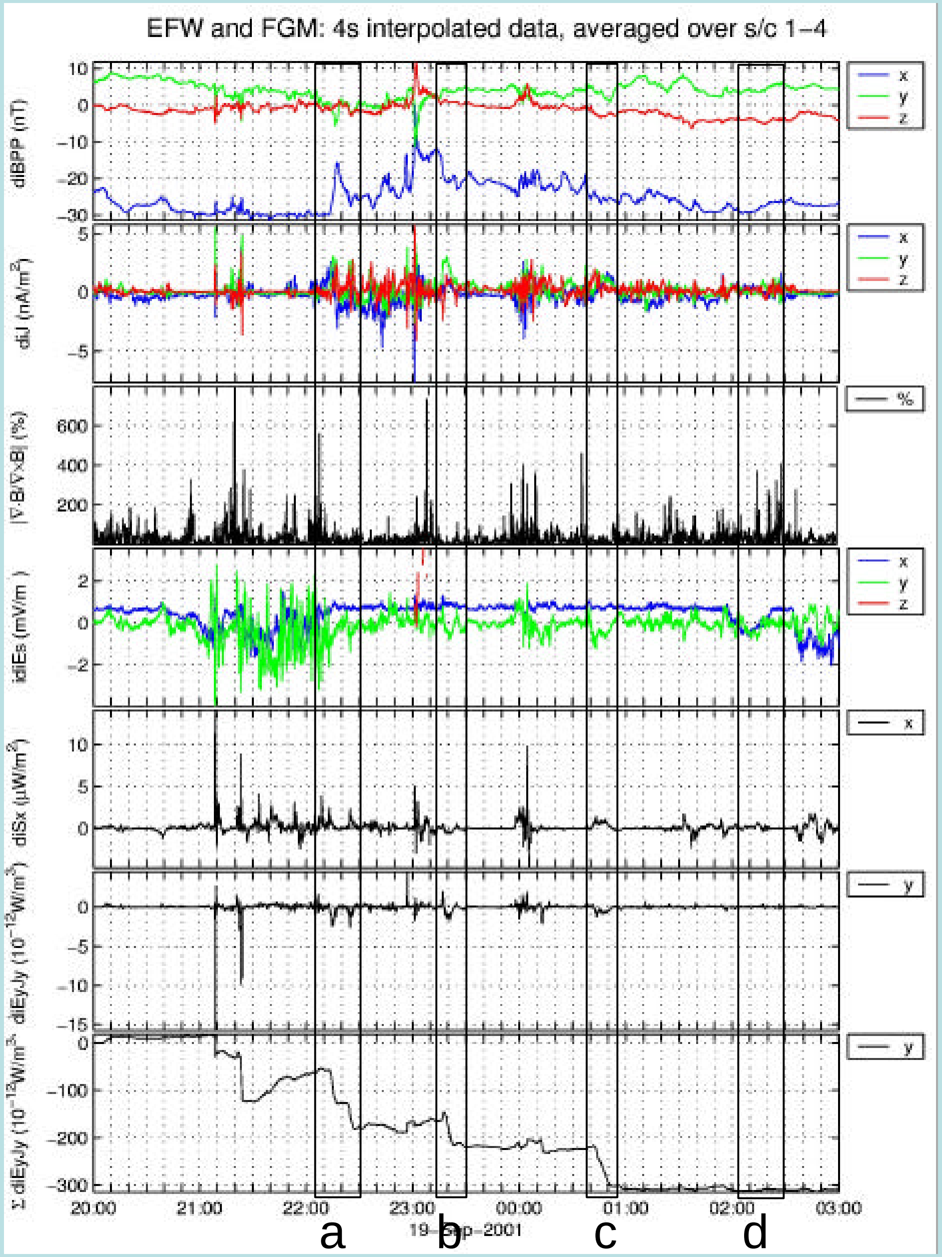

EFW and FGM: 4s interpolated data, averaged over s/c 1−4
diBPP (nT)
diJ (nA/m²)
|∇·B/∇×B| (%)
idiEs (mV/m)
diSx (μW/m²)
diEyJy (10⁻¹²W/m³)
Σ diEyJy (10⁻¹²W/m³)
x
y
z
%
20:00
21:00
22:00
23:00
00:00
01:00
02:00
03:00
19−Sep−2001
a
b
c
d

G2

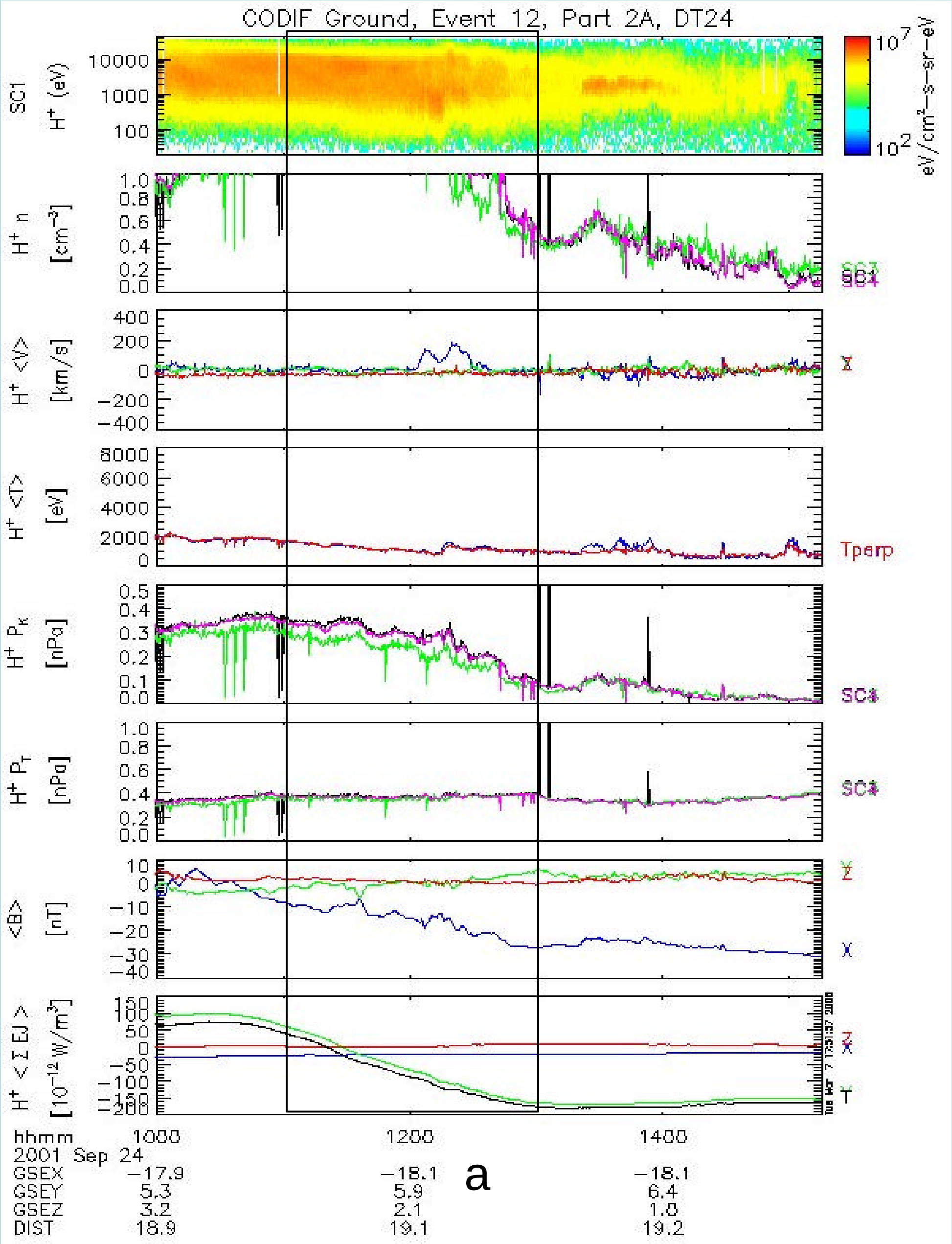
CODIF Ground, Event 12, Part 2A, DT24
hhmm 1000 1200 1400
2001 Sep 24
GSEX −17.9 −18.1 −18.1
GSEY 5.3 5.9 6.4
GSEZ 3.2 2.1 1.8
DIST 18.9 19.1 19.2

a

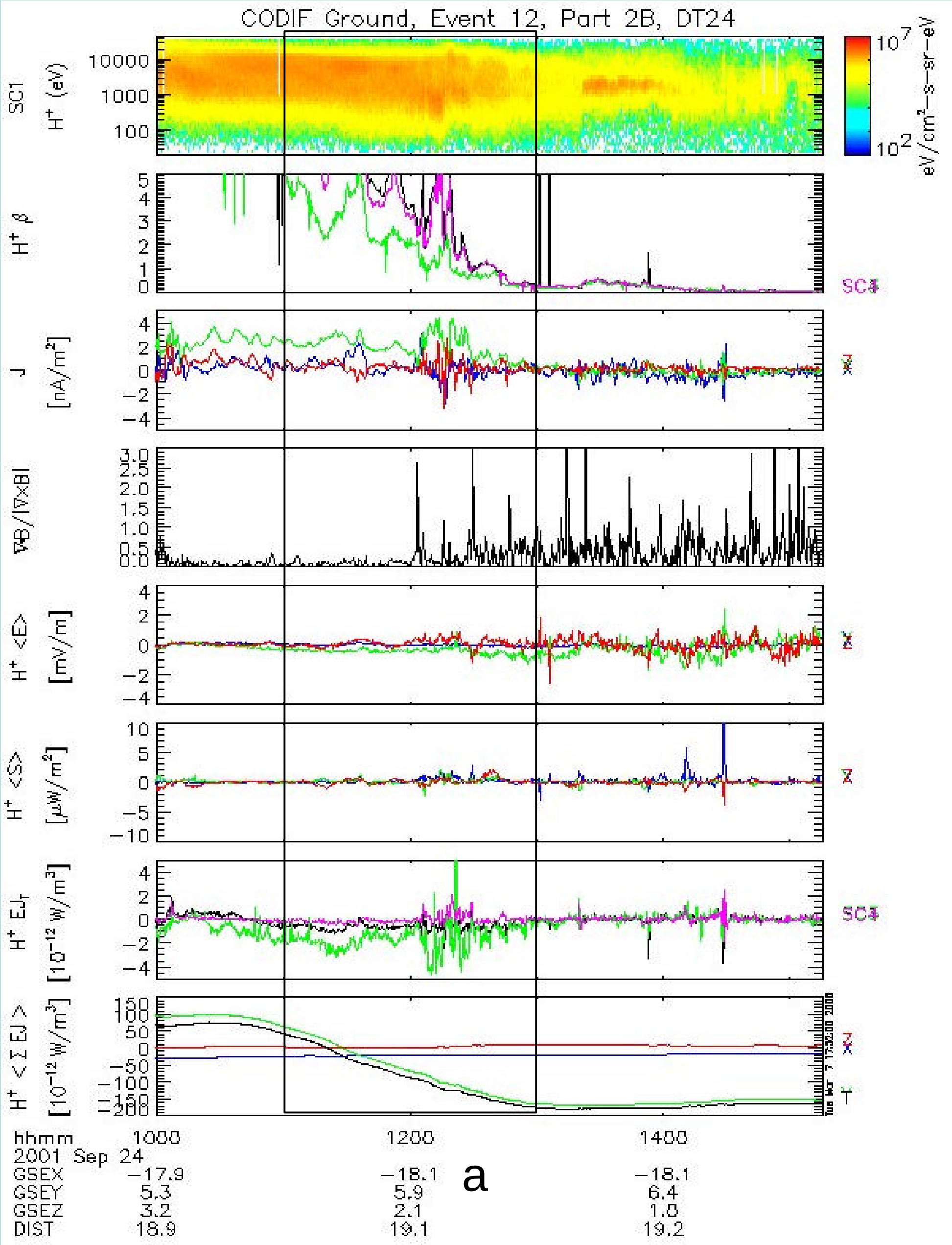
CODIF Ground, Event 12, Part 2B, DT24
hhmm 1000 1200 1400
2001 Sep 24
GSEX −17.9 −18.1 −18.1
GSEY 5.3 5.9 6.4
GSEZ 3.2 2.1 1.8
DIST 18.9 19.1 19.2

a

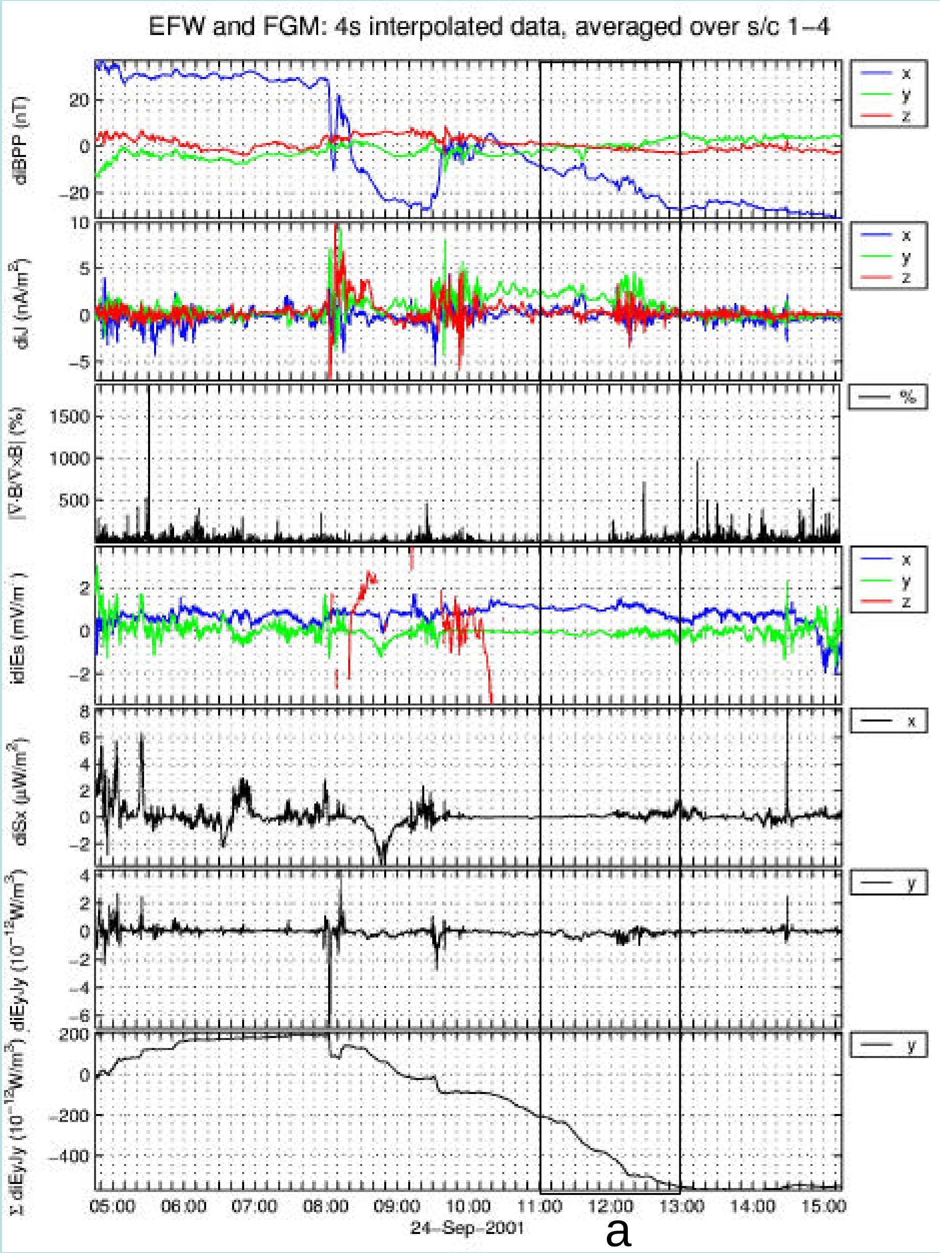
EFW and FGM: 4s interpolated data, averaged over s/c 1−4
diBPP (nT)
diJ (nA/m²)
|∇·B/∇×B| (%)
idiEs (mV/m)
diSx (μW/m²)
diEy.Jy (10⁻¹²W/m³)
Σ diEy.Jy (10⁻¹²W/m³)
05:00
06:00
07:00
08:00
09:00
10:00
11:00
12:00
13:00
14:00
15:00
24−Sep−2001
a

Simulation results, Birn and Hesse (BH), 2005

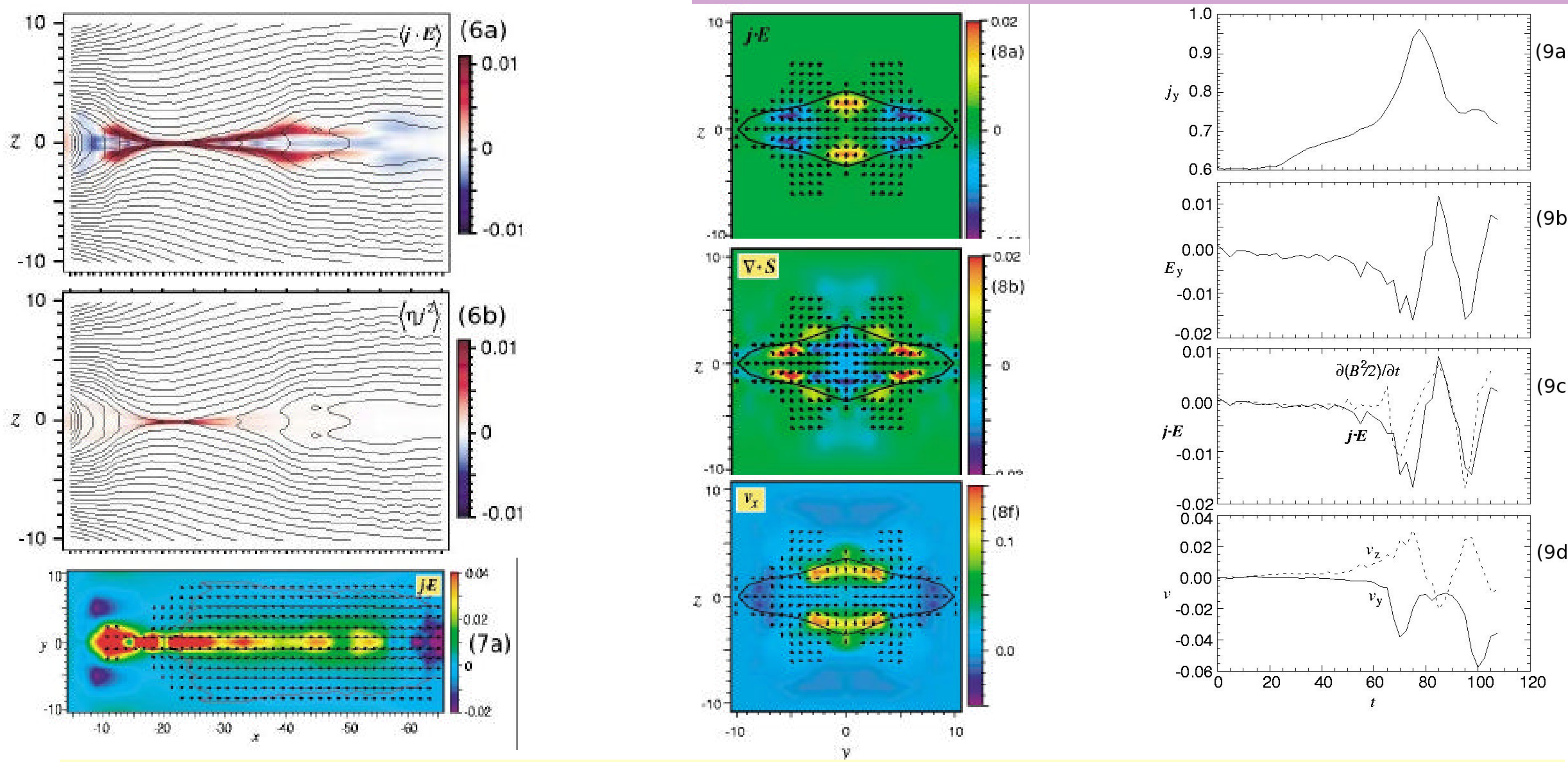

Selection of energy conversion features from BH 2005, Figs. 6, 7, 8, 9 (simulation units: L=6000–12000 km, t=6–12 s, v=1000 km/s, B=40 nT).

Left: Energy conversion terms integrated over y (6a, 6b) and over z (7a).

Center: Characteristic quantities near the conversion regions, at x=-8.75 and t=100.

Right: Characteristic quantites in the generator region, at x=-8.75, y=-4, z=1.2.

Good agreement data vs. simulations:

- The energy conversion regions (ECRs) have mostly load character.
- Association of the ECRs with bulk flow.
- Integrated load close to midnight.
- Integrated generators on the sides.
- Energy conversion near the plasma sheet boundary.
- Net Poynting flux from the generator regions.
- Few minutes ECR time scale.

Summary

- The investigation method, initially developed to search for generator regions, allows a systematic examination of the local energy conversion between electromagnetic and mechanical – in both generator and load regions.
- Cluster North–South crossings of the plasma sheet show, on large scales, mostly load character, with a substantial fraction of the load near the neutral sheet.
- The magnitude of the integrated load seems to decrease from midnight to the dusk. Away from the midnight one can even encounter large scale generator regions, in good agreement with simulation results,
- On small scale, both concentrated load regions (CLRs) and concentrated generator regions (CGRs) are seen. The CGRs seem to develop more often in the PSBL, as inferred from the plasma b parameter – consistent, again, with the simulations. High power density CLRs are located not far from the neutral sheet, in high b plasma, while for the low/moderate power density CLRs a clear dependence on b it is not obvious.
- The concentrated energy conversion is related to bulk plasma flow, dominantly along the magnetic field – also seen in the simulations. Temperature anisotropy is observed as well, with Tpar > Tperp.

Prospects and Open Questions

• Closer look at the local energy budget – work of the pressure forces, Poynting theorem, …

• Cross-check of **J** by (rough) comparison with ∇ P.

• Completing the dawn–dusk survey with the Cluster plasma sheet crossings in June – August 2001.

• Integrated load / generator character versus Y_{GSE} (the distance form the midnight), and versus AE.

• Is the plasma flow associated with local acceleration and parallel electric fields? Is the anisotropy related to thermalization, achieved faster in parallel direction ?

• Reversible versus irreversible processes – entropy calculation?

• Cluster plasma sheet crossings in 2002 – 2004.

• Energy conversion at the magnetospheric flanks => better electric field from EFW, as well as EDI.

• Also close to the subsolar point, later in the mission?

• Extension to THEMIS and MMS?

References

• Birn and Hesse, Energy release and conversion by reconnection in the magnetotail, 23, 3365 – 3373, 2005.

• Hamrin et al., Observations of concentrated generator regions in the nightside magnetosphere by Cluster/FAST conjunctions, Ann. Geophys., 24, 637 – 649, 2006.

• Marghitu et al., Experimental investigation of auroral generator regions with conjugated Cluster and FAST data, Ann. Geophys., 24, 619 – 636, 2006.